This manuscript was published in Wireless Personal Communication

The final publication is available at link.springer.com

https://link.springer.com/article/10.1007/s11277-016-3653-6

Body Attenuation and Path Loss Exponent Estimation for RSS-Based Positioning in WSN

Helder D. Silva[1], Jose A. Afonso[2], Luis A. Rocha[3]

***Abstract*—The influence of the human body in antenna systems has significant impact in the received signal strength (RSS) of wireless transmissions. Accounting for body effect is generally considered as being able to improve position estimation based on RSS measurements. In this work we perform several experiments with a wireless sensor network, using a sensor node equipped with an inertial measurement unit (IMU), in order to obtain the relative orientation between the sensor node and multiple anchor nodes. A model of the RSS attenuation induced by the body was created using experimental measurements in a controlled environment and applied to a real-time positioning system. A path loss exponent (PLE) estimation method using RSS information from neighbor anchors was also implemented and evaluated. Weighted centroid localization (WCL) algorithm was the positioning method used in this work. When the sensor node was placed on the user's body, accounting for body effect produced negligible improvements (6%) in the best-case scenario and consistently degraded accuracy under real conditions, whether the node was placed on the user's body (in the order of 3%), 10 cm away (from 14% to 35%) or 20 cm away from the body (from 42% to 105%) for results in the 70th percentile. The PLE estimation method showed improvements (in the order of 11%) when the sensor node is further away from the body. Results demonstrate that the distance between sensor node and the body has an extremely important influence on the accuracy of the position estimate.**

***Index Terms*— Received signal strength, body effect, propagation model, wireless sensor networks, positioning, CRLB.**

Helder D. Silva (Corresponding author)
CMEMS-UMinho, University of Minho - Campus of Azurem, 4800-058
Guimaraes, Portugal. Email: helderdavidms@gmail.com
Phone: +351 253 510 190, Fax: +351 253 510 189
Jose A. Afonso
CMEMS-UMinho, University of Minho – Campus of Azurem, 4800-058
Guimaraes, Portugal. Email: jose.afonso@dei.uminho.pt
Luis A. Rocha

CMEMS-UMinho, University of Minho – Campus of Azurem, 4800-058
Guimaraes, Portugal. Email: lrocha@dei.uminho.pt

1 INTRODUCTION

The internet of things (IoT) is a vision consisting of a world where a large number of common objects used in a daily basis are imbued with computational and communication capabilities, efficiently automating innumerous tasks [1]. This vision is closely related to the ubiquitous computing vision from Mark Weiser, in which "technologies disappear into the background", facilitating daily tasks [2]. There are several institutions working in order to achieve this vision, not only in the form of standards creation and improvement, but also in the interaction between different standards, so a global network augmented by these objects can be realized [3]. Sensor networks have a central role in this ubiquitous computing vision, since they provide the connection to the real world through sensors and actuators. A plethora of different sensors can be applied to the most diverse scenarios and the information generated by these sensors can be used to achieve higher understanding or process efficiency.

The terms IoT and ubiquitous computing, along with other terms such as ambient intelligence, pervasive computing and smart objects are related and sometimes used interchangeably in literature. A common feature shared between these visions, directly related to the data sensed from these smart objects, is the location from where the data is collected. Positioning technology is a key enabler for the ubiquitous computing vision due to the application opportunities that arise with the knowledge of the position of the user or device. In this work, the focus is on positioning capabilities in wireless sensor networks (WSN) applied to indoor environment, which is a major component of the ubiquitous computing vision.

WSN nodes are sensing capable devices composed by a microcontroller and a wireless transceiver. WSN constraints nowadays relate to device cost, energy and computational capabilities, the latter of which trades-off with higher battery recharge frequencies. Positioning in WSN can be accomplished by using optical, acoustic or radio frequency (RF) technologies, to produce range, angle or pattern information. Using one of these measurements, or a combination of them, the location of a device can be computed.

Ultrawideband (UWB) is a technology that enables ranging capabilities between devices and allows the detection of multipath components of transmitted signals by using large channel bandwidths. This technology holds the key to solve indoor positioning systems due to its sub-meter ranging accuracy. Yet, due to the existence of two versions of UWB standard competing among each other, a pulsed version and a frequency division version, standard acceptance has been very slow. Furthermore, the ranging capability feature is optional, not obligating manufacturers to implement it in order to comply with the standard. Due to the slow standard acceptance, there isn't yet a mass market in place, which in turn affects device cost for currently available off-the-shelf components. The inclusion of UWB in IEEE 802.15.4 standard [4] as a low power physical layer is a step towards faster industry acceptance, due to the popularity of 802.15.4 and its network and application layer protocol ZigBee.

RSS positioning stands as a fast and inexpensive method to obtain localization services in WSN, with accuracies spanning from 3 to 10 meters. With higher accuracy, this localization technology could deliver the quality of service necessary for wider range of IoT applications. Low power consumption is a typical requirement in WSN, since nodes are usually battery operated. A WSN node is capable of RSS positioning without the addition of extra hardware, thus not incurring in additional energy consumption. Coexistence with other systems, objects and environment is an important aspect of positioning systems. Coexistence with the users in RSS positioning is especially important due to the body influence in RSS readings.

The effect of the body on the propagation conditions is an important topic for communications systems deployment and performance assessment. The proximity of the human body is an important factor which induces bias in the position estimation, with attenuations as high as 15 dB under non-line-of-sight (NLOS) conditions [5]. When the user's body blocks the LOS transmission between two devices, a part of the wave travels through the body (shadow fading occurs) while the remaining wave energy is absorbed, reflected, diffracted and scattered. These attenuation effects directly influence RSS positioning algorithms since RSS is used to infer distance.

Some works attempt to model body effect in the antenna using the super-antenna concept referred in [6], which is directly related to shadowing caused by the proximity of the body. In this model, the body is considered as an integral part of the antenna, contributing to the radiation diagram. Besides radiation pattern, factors such as transmission power and radio frequency also play an important role [7].

The sparse anchor problem [8] is also an issue for localization algorithms in WSN since a minimum number of anchors are needed to provide a location estimate. If enough anchors are available, the positioning estimate is also dependent on the anchor placement in the field. This problem is known as geometric dilution of precision (GDOP) and happens when anchor locations are collinear [9].

The work presented in [10], where a model of relative antenna gain versus rotation is inferred from measurements, also considers body effects. This antenna gain model is used in conjunction with an inertial model, which assumes the orientation of the user is the same as the orientation of its velocity vector. In [5] the body effect is characterized in terms of the location of the sensor node (pocket or necklace), contact time and effective bandwidth between sensor nodes both in indoor and outdoor environments. The work in [11] encountered variations of up to 30 dB when the source is located from 0 cm to 10 cm off the body. Body posture and antenna placement in the user's body is analyzed in [12], where body movement is of utmost importance for the communications performance.

In practical situations, indoor conditions and the proximity of the user's body significantly hinder the propagation model's correlation with distance. Furthermore, RSS variance only occurs when the environment is dynamic, e.g. when any surrounding objects or transmitter and receiver devices are moved. When every object and both transmitter and receiver devices are static, the multipath effect does not change in time, and the RSS is given by the sum of all copies of the original signal that the receiver can detect [13]. For example, a receiver placed 10 m away from a transmitter will experience the

same RSS variance as when the receiver is placed 2 m away from the transmitter. This variance property is what enables tomographic radio imaging systems to track user movements inside buildings [14]. Since the variance of the signal is small under static conditions, averaging over time will not influence the outcome of the positioning error. This implies that the RSS received by the device in static conditions is a function of constant multipath and shadowing effects that are occurring in a given instant. When the user moves or the environment changes (e.g. a door opens), these multipath and shadowing effects also change, thus the RSS variance is both position and environment dependent [13].

In this paper the localization accuracy of RSS based methods is studied in indoor environments, using a WSN based on the IEEE 802.15.4 medium access control (MAC) protocol in the 2.4 GHz frequency band. This work builds on top of a previous work [15], where a comparison between different RSS based algorithms was performed in a controlled and predefined indoor environment. In this work the same indoor environment is used and extends the previous work by using inertial and magnetic sensor information to infer the orientation of the user's body. Since the user's body is the only LOS blocking source in the experimental setup, by inferring its orientation, the anchor nodes that possess line-of-sight (LOS) communication with the sensor node are effectively identified. A body attenuation model is then used to compensate the RSS of each anchor node, according to the orientation of the user relative to the anchor node. Furthermore, RSS information broadcasted by each anchor node is also used, in order to estimate in real-time the path loss exponent (PLE) affecting the positioning scenario. The weighted centroid localization (WCL) was chosen in this work as the positioning algorithm, since it provided the best results in the previous work [15]. The performance of WCL based positioning algorithms is then evaluated to assess the effect produced by incorporating the body effect and the PLE estimation into the localization algorithm.

The paper is organized as follows: Section 2 provides background information on RSS positioning methods, along with issues associated with RSS positioning. Section 3 describes the materials and methodology used to experimentally assess the body effect in WCL based positioning algorithms. Section 4 presents the results obtained, which are followed by a brief discussion in Section 5. Conclusions of the work are drawn in Section 6, along with further work to be developed.

2 BACKGROUND

Hybrid positioning techniques are a popular research topic in WSN, due to devices combining a radio interface along with sensing capabilities. Data is gathered from several sensors and fused with RSS positioning techniques in order to improve accuracy [16]–[18]. There are three methods in which RSS can be used to infer location: using RSS as a measure of proximity [19], [20]; using propagation models which translate RSS to distance [21], [22]; or by creating a RSS map from multiple base stations or access points [23]–[25]. These methods have been extensively studied in the literature, and several implementations using these concepts exist. Accuracy from these methods is directly related to RF propagation, depending on features like the topology of a building, construction materials, objects, furniture and number of persons inside a room.

When propagation models are used, the PLE is usually considered fixed for a specific scenario. This is also one of the main problems, since the PLE is a key parameter in distance estimation which varies with position and environment changes [22]. According to [26] a fixed environment-dependent PLE generally has smaller variance compared to the dynamic PLE obtained through an estimation process, which demonstrates the random nature associated with the propagation environment. PLE estimation suffers from multipath and shadowing effects, which are the main sources of error in RSS based positioning systems, especially in indoor environments. Multipath happens when the radio wave travels the propagation medium interacting with objects along the way, suffering attenuation, reflection, scattering and diffraction [27]. Multiple copies of a signal arrive at the receiver with different attenuations, delays and phase-shifts, which are added constructively or destructively depending on each signal phase. The multipath effect depends on the number of objects, dimensions and dielectric material properties present in the signal's propagation path. This effect is also commonly termed small-scale effect or fast fading [13], due to the fast RSS variations over small distances (in the order of the wavelength).

Shadowing happens when the radio wave travels through different obstacles or mediums, suffering attenuation in the process [28]. Shadowing and path loss (the gradual decay of signal power along distance) are also called large-scale effects or slow fading, due to the slower RSS variations over greater distances. These large-scale effects are always present whether static or dynamic scenarios are considered. For greater distances between transmitter and receiver, the probability of the signal encountering a greater number of objects is also higher, thus it is common to find in literature increasing variances for higher distances between devices.

Ray-tracing techniques are a common tool used in network planning and deployment, in order to determine efficient device placement in a building [29]. This type of tool can generate a map of radio propagation, which can be used in producing more accurate distance estimates. Due to the dynamics of indoor environments, it is unfeasible to have a radio map being constantly updated by a ray-tracing algorithm and deployed to devices in a particular room.

RSS dependence on the environment is what makes indoor positioning a challenging task, due to the accuracy of the position estimate being a function of so many variables, which can vary widely from one indoor scenario to another. In practice, since indoor propagation environment complexity is very high, an empirical model such as the One-Slope model is used extensively [27]. It is a simple model that captures the essence of the signal decay with distance (d), incorporating the shadowing effect by using a zero-mean Gaussian random variable:

$$P_R(d) = P_0 - 10 \cdot n \cdot log\left(\frac{d}{d_0}\right) + X_\sigma \qquad (1)$$

where P_0 is the RSS received at the reference distance d_0 (usually assigned to 1 m), n is the PLE and χ_σ is the Gaussian random variable. Note that by using the constant power at the reference distance, we are indirectly stating that the transmission power is fixed and known.

The Cramer-Rao lower bound (CRLB) is often used in literature to describe a positioning system's best attainable accuracy, by providing a lower bound on the variance of a location estimator. This can be used not only as a benchmark for accuracy assessment of a particular positioning algorithm, but also to provide insight on the behavior of the accuracy when parameters of the model change [30]. The bound is given by:

$$CRLB \geq \frac{1}{-E\left[\frac{\partial^2}{\partial\theta^2} ln(p(X;\theta))\right]} \qquad (2)$$

where E is the expected value, X is the random measurement and θ the parameter to be estimated from the measurement.

In [31], [32], theoretical accuracy bounds are studied for RSS positioning, which for a single RSS reading is given by:

$$\sqrt{Var(d)} \geq \frac{\sigma \cdot d}{10 \cdot n \cdot log(e)} \qquad (3)$$

where d is the distance between transmitter and receiver, n is the PLE, e is the Euler number and σ is the standard deviation of the shadowing effect from equation 1. This theoretical framework allows insight over the properties that affect accuracy. From equation 3 we can denote that RSS variance increases with the distance, such as reported in [20], [30], [33]–[36], and decreases with increasing PLE n, such as observed in [15]. The bound itself may be unachievable yet it serves as an overall accuracy mark that positioning algorithms can be compared to.

3 Materials and Methods

3.1 Hardware

The hardware used in this work is based on Texas Instruments CC2530 system on chip using the Antenova M2M 2.4 GHz swivel antenna [37]. Two extra boards were added to the sensor node, one board containing the battery and the sensor platform (containing inertial and magnetic sensors, such as the sensor node described in [38]), and another board containing a secure digital (SD) card to store data. These boards are interconnected through 20-pin header connectors, allowing a modular approach for rapid prototyping.

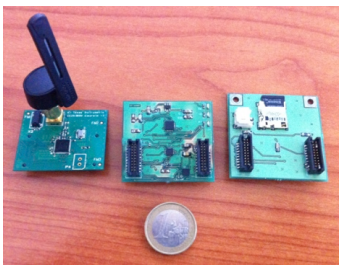

Figure 1: Sensor node prototype. The CC2530 module is shown on the left, the sensor and battery board in the middle and the SD card board on the right.

The sensor platform integrates an InvenSense MPU6000 with a Honeywell HMC5883L. The MPU6000 embeds an accelerometer, a gyroscope and allows integration with an external sensor via I2C protocol. The noise values are 0.005 °/s

and 400 µg at 10 Hz for the gyroscope and accelerometer respectively. The HMC5883L magnetic sensor noise is 5 milli-gauss. The MPU6000 collects samples from each sensor and stores them in a first-in-first-out (FIFO) buffer. A sampling frequency of 100 Hz is used, which means that at every 3 samples from the MPU, the magnetic sensor outputs a repeated sample due to its maximum sampling frequency of 75 Hz. The data stored in the FIFO from all three sensors are read using the Serial Peripheral Interface (SPI) protocol in a single burst at a 1 MHz clock frequency, using the serial port and the direct memory access (DMA) controller from the CC2530.

This sensor setup, referred to as inertial measurement unit (IMU) from now on, allows the determination of device orientation. The data collected from RSS and IMU is stored in a file on the SD card for offline processing in MATLAB.

A CC2530 module, with the same antenna as the sensor node, is used in the anchor nodes. The CC2530 module is mounted on a battery board from the Texas Instruments CC2530 development kit and is powered using two AA batteries.

3.2 Orientation Measurement

Only the accelerometer and magnetometer sensor data is used to determine orientation in this work. Prior to measuring orientation, a calibration procedure is performed to compensate for offsets in the sensors. The minimum and maximum value of each axis is obtained by manually aligning the sensing axis with gravity, for the calibration of the accelerometer, and the magnetic north for the calibration of the magnetometer. The minimum and maximum values are then used in equation 4 to produce uniform values from -1 to 1:

$$u = \frac{Reading - Min}{\frac{Max - Min}{2}} - 1 \qquad (4)$$

A tilt-compensated e-compass method using rotation quaternions was implemented to determine orientation. Figure 2 depicts the right-handed sensor coordinate system used in the IMU.

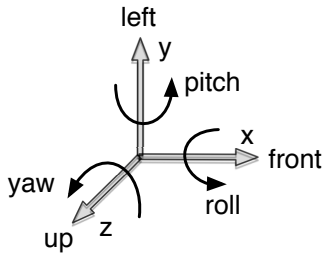

Figure 2: Sensor coordinate system.

The orientation measurement consists in finding the Euler angles (*roll*, *pitch* and *yaw)* between the sensor coordinate system and the global coordinate system, where gravity is aligned with the –*z*-axis and the projection of the magnetic north in the azimuth plane is aligned with the +*x*-axis. First the *roll* and *pitch* angles are computed with the accelerometer data, using equations 5 and 6:

$$roll = tan^{-1}\left(\frac{-g_y}{-g_z}\right) \qquad (5)$$

$$pitch = tan^{-1}\left(\frac{g_x}{\sqrt{g_y^2+g_z^2}}\right) \qquad (6)$$

where g_x, g_y and g_z are the normalized gravity vector components, which are measured by the accelerometer sensor when there are no external forces acting on the sensor node. Using the *atan2* and *atan* methods in MATLAB for *roll* and *pitch* angles respectively produces angles in canonical form. *Roll* varies between ±180º and *pitch* varies between ±90º. Two rotation quaternions are created using equations 7 and 8, for the *roll* and *pitch* angles obtained from the accelerometer readings.

$$\mathbf{{}^{b}_{w}q_{roll}} = \left(cos\frac{roll}{2}, sin\frac{roll}{2}, 0, 0\right) \qquad (7)$$

$$\mathbf{{}^{b}_{w}q_{pitch}} = \left(cos\frac{pitch}{2}, 0, sin\frac{pitch}{2}, 0\right) \qquad (8)$$

The notation $\mathbf{{}^{b}_{w}q}$ denotes the quaternion $\boldsymbol{q}$ that rotates from the body frame (*b*) to the world frame (*w*) (or inertial frame) aligned with the gravity and the magnetic north vectors. The tilt rotation quaternion is computed by simply multiplying the *pitch* and *roll* quaternions.

$$\mathbf{{}^{b}_{w}q_{tilt}} = \mathbf{{}^{b}_{w}q_{roll}} \times \mathbf{{}^{b}_{w}q_{pitch}} \qquad (9)$$

The *yaw* angle is computed by first applying the tilt rotation, which brings the magnetic vector (**m**) into the azimuth plane:

$$\boldsymbol{h} = \mathbf{{}^{b}_{w}q_{tilt}} \times (0, \boldsymbol{m}) \times \mathbf{{}^{b}_{w}q^{*}_{tilt}} \qquad (10)$$

where the magnetic vector (**m**) is converted to a quaternion with scalar part equal to zero. The *yaw* angle is then computed using equation 11:

$$yaw = tan^{-1}\left(\frac{-h_y}{h_x}\right) \qquad (11)$$

where h_x *and* h_y are the normalized rotated version of the magnetic vector components. The *yaw* angle is computed using the *atan* method and varies between ±180º. Finally a rotation quaternion is created using half of the *yaw* angle:

$$\mathbf{{}^{b}_{w}q_{yaw}} = \left(cos\frac{yaw}{2}, 0, 0, sin\frac{yaw}{2}\right) \qquad (12)$$

Multiplying the *yaw* quaternion by the tilt quaternion produces the full orientation of the sensor node in quaternion format:

$$\mathbf{{}^{b}_{w}q_{f}} = \mathbf{{}^{b}_{w}q_{tilt}} \times \mathbf{{}^{b}_{w}q_{yaw}} \qquad (13)$$

3.3 Path Loss Exponent Estimation

When deploying a WSN in an indoor environment, PLE estimation is accomplished by performing several power measurements at different distances from a transmitting node. These measurements are then used to compute a best-fit constant value for the PLE parameter, to be used in the positioning area. This task was also performed in [15] for our

experimental setup. In this work a different approach is explored, which uses the distance information that is configured in the anchor nodes of the positioning system. Given that each anchor is assigned a location, distances between anchors are known. Since nearby anchor nodes also receive the beacons broadcasted, a PLE estimate can be obtained from this information.

In [15] anchor nodes are configured to send beacon messages periodically (100 ms superframe). The anchor nodes in this work are configured to additionally include RSS information from other anchor nodes in the beacon messages. During a superframe, the sensor node receives one beacon message from each anchor node, with each beacon message containing a list of RSS readings that the respective anchor node received from other anchor nodes in communication range. With RSS and distances between anchor nodes, PLE estimation for each link is obtained using equation 14, which is derived from equation 1:

$$n = \frac{R_A - P_0}{-10\, log_{10}(d)} \qquad (14)$$

where R_A is the RSS received by the anchor node for a specific link and P_0 is the RSS at the reference distance of 1 meter. Assuming that all four anchor nodes from our positioning scenario have full connectivity, each anchor will capture RSS from all other three anchors and broadcast this information in the beacon message. The sensor node uses this information to infer the PLE for each anchor. Figure 3 depicts an iteration of the algorithm, referred to as closest links path loss (CLP).

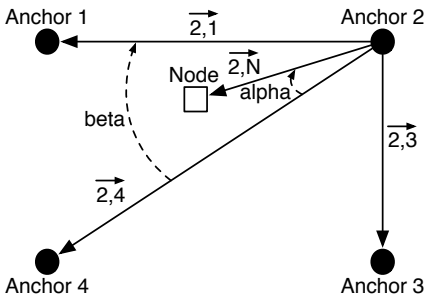

Figure 3: Closest links path loss algorithm iteration example for anchor 2

First the sensor node computes the initial position estimate using the RSS received from the anchor nodes using WCL algorithm. This initial position estimate, together with the known anchor coordinates is used to find the node and anchors displacement vectors (vectors 2,1 2,N 2,3 and 2,4 in Figure 3). Using the cross product rule with the *z* component set to 0, the area of the parallelograms formed by each anchor displacement vector and the node displacement vector are computed. The two smallest areas are chosen, which correspond to the links closer to the node's initial position estimate. Next, a linear interpolation is used to find the PLE of the sensor node's link to the anchor, by using the angle between the two closest links (beta angle) and the angle between one of the links and the user displacement vector (alpha angle). The angles are computed using the dot product and a linear interpolation is used to find the PLE using equation 15.

$$n = n_{i,1} \times \frac{\beta - \alpha}{\beta} + n_{i,2} \times \frac{\alpha}{\beta} \qquad (15)$$

where $n_{i,1}$ and $n_{i,2}$ are the PLEs of the closest links to the node's estimated position, beta is the angle between the closest links, and alpha is the angle between one of the closest links and the user displacement vector. This PLE (n) represents the state of link attenuation from the previous superframe, and allows estimation of the distance between the sensor node and the respective anchor node by using equation 16, which is derived from the One-Slope model of equation 1:

$$d = 10^{\left(\frac{R_S - P_0}{-10n}\right)} \qquad (16)$$

where R_s is the RSS received by the sensor node, P_0 is the RSS at the reference distance and n is the PLE obtained from equation 15. This procedure is repeated for each anchor node, and the distances obtained for each anchor are then used in the WCL algorithm to estimate the position of the sensor node.

The goal associated with this procedure is to use as much RSS information as possible, in order to capture PLE changes caused by the user's body or the moving environment.

3.4 Evaluation of Body Effect in RSS

Body effect experiments were carried out in two different environments, a positioning area of 4.7 m by 10 m (approximately 50 m^2) and an anechoic chamber. More details regarding the positioning area can be found in [15]. Figure 4 details the anechoic chamber setup.

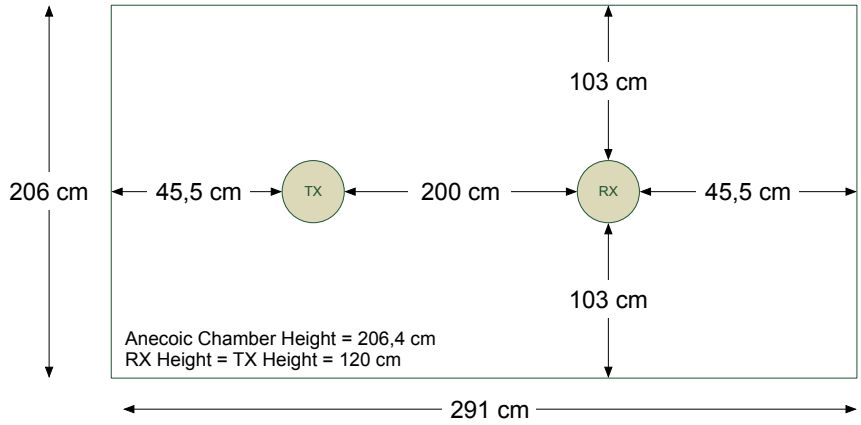

Figure 4: Anechoic chamber setup

To evaluate body effect on RSS, three sets of measurements were collected: static with body influence (case 1), where the device is placed on the user's body while the user is standing still; static without body influence (case 2), where the device is placed on top of a plastic stand; and dynamic (case 3), where the device is placed on the user's body and the user performs a 360º rotation. For all scenarios the device is always placed at waist level, 1.2 m above the ground. The goal is to distinguish between device effects (hardware effects such as antenna placement in the device and radiation pattern) and body effects, as well as between static and dynamic situations.

The anechoic chamber tests provide a controlled environment without external interferences. It enables determination of the multipath and shadow fading caused by the body alone, since other multipath components from wall and ground reflections

are severely attenuated or non-existent in this type of environment. The positioning scenario tests provide real data for comparison with controlled environment data.

Data capture is accomplished by the sensor node, which receives messages from a transmitter node placed at the same height and at a distance of 2 m. The sensor node simply stores the RSS values from the received messages and the raw IMU data in a file on the SD card.

3.5 Attenuation Model

The RSS received by the sensor node from each anchor node is influenced by the user's orientation according to an attenuation model that relates the relative attenuation with the user's orientation. First, a reference orientation relating the positioning setup coordinate system to the global coordinate system is required (e.g. the positioning setup coordinate system offset relative to the magnetic north). This reference orientation was initially measured in our positioning scenario. To find the relative angle between the user's orientation and an anchor node, the user location on the positioning scenario is also needed. If the WCL algorithm is used to find this position, an additional error is added in the relative angle estimation and therefore, to avoid this additional error, the real position logged during the data collection phase, such as in [15], is used in order to compute the anchor direction. This allows the inclusion of orientation information with a much smaller error than using WCL to find position, which can be seen as a best-case scenario where orientation information is the best possible.

Anchor direction relative to the sensor node is found using equation 17, by computing the vector difference between the location of the sensor node ($\boldsymbol{p_s}$) and the location of the anchor node ($\boldsymbol{p_a}$).

$$\boldsymbol{a} = \boldsymbol{p_s} - \boldsymbol{p_a} \qquad (17)$$

The orientation of the sensor node is corrected by multiplying the IMU orientation quaternion by the quaternion representing the north offset angle, measured in the positioning setup coordinate system using equation 18.

$$\boldsymbol{{}^{b}_{w}q_c} = \boldsymbol{{}^{b}_{w}q_{imu}} \times \boldsymbol{{}^{b}_{w}q_{offset}} \qquad (18)$$

With both the world (inertial) coordinate frame and the local coordinate frames of the positioning area aligned, the sensor node's forward direction is obtained by multiplying the resulting rotation quaternion by a 3D vector pointing in the *x*-axis direction (i.e. 0º roll, 0º pitch and 0º yaw), using equation 19:

$$\boldsymbol{b} = \boldsymbol{{}^{b}_{w}q_c} \times (0, \boldsymbol{d}) \times \boldsymbol{{}^{b}_{w}q_c^*} \qquad (19)$$

where $\boldsymbol{d}$ is a quaternion with zero scalar part and vector part equal to the *x*-axis direction (e.g. vector [1,0,0]) and $\boldsymbol{{}^{b}_{w}q_c^*}$ is the quaternion conjugate. The scalar part of quaternion $\boldsymbol{b}$ from equation 19 is discarded and the 3D orientation vector is given by the vector part. We are only interested in the *yaw* component of the orientation, since the attenuation model is created only in the azimuth plane. Discarding the *z* component of the 3D vector representing the sensor direction, the relative angle between sensor and anchor direction is simply given by the angle between two vectors:

$$\alpha = cos^{-1}\left(\frac{\boldsymbol{a}\cdot\boldsymbol{b}}{\|\boldsymbol{a}\|\cdot\|\boldsymbol{b}\|}\right) \quad (20)$$

$$\boldsymbol{r} = \boldsymbol{a}\times\boldsymbol{b} \quad (21)$$

Vectors $\boldsymbol{a}$ and $\boldsymbol{b}$ represent anchor direction and sensor direction respectively. Since the angle will always be the smallest angle between both vectors, multiplying the angle by the sign of the rotation axis produces absolute orientation. The angle produced by equations 20 and 21 are used to lookup the attenuation value of the model collected in the anechoic chamber. A linear interpolation is used when no information is available for the angle detected by the sensor node (e.g. between two points in the attenuation model).

4 RESULTS

This section presents the results for the experiments carried out in the proposed scenarios. The reader interested in a benchmark between RSS-based algorithms in the experimental environment of this work can resort to [15]. RSS data collected to study the body effect is presented in polar plots. Units for RSS data are dBm and angles are in degrees. Regarding positioning algorithm performance, the parameters found in [15], which maximize WCL accuracy, were used as default parameters in this work. When using the raw RSS readings for WCL, the exponent *e* was set to 3.4 (same as RWCL in [15]). For distances (obtained from the One-Slope model) used as weights in CLP, the exponent *e* of 1 and the reference power P_0 of -37.72 were used (same as DWCL in [15]). The performance indicator chosen is the Euclidean distance between real position and estimated position. Cumulative distribution functions and geographical error distributions are presented for each algorithm, with and without body effect compensation.

4.1 Analysis of Body Effect in RSS

Due to blockage of the Earth's magnetic field inside the anechoic chamber, a manual orientation measurement was performed by means of markers placed in the floor. For the positioning scenario, orientation was obtained using the IMU after performing the calibration procedure. The sensor node was either fitted to the user at waist level in case 1 (static with body influence) and case 3 (dynamic with body influence) or placed on top of a plastic stand in case 2 (static without body influence) at the same height (1.2 meters) as the user's waist. Rotations were performed along the vertical axis (*z*-axis) in a counter-clockwise direction, with 0º being the orientation facing the anchor node (LOS) and 180º being the opposite direction (NLOS). Due to space constraints inside the anechoic chamber, the distance between sensor and anchor nodes was fixed to 2 meters in both test scenarios. For cases 1 and 2, the sensor node was oriented accordingly, and 100 RSS samples were collected. For case 3, the user performs a 360º turn during approximately 60 seconds. Since the sensor was placed at waist level, some interference was expected due to the user's arms (cases 1 and 3). The user's arms were in a resting position along the torso. Results are summarized in Figure 5, where the absolute value of RSS is presented. The body effect experiments in the positioning scenario were performed with a minimum distance to the walls of 2 meters.

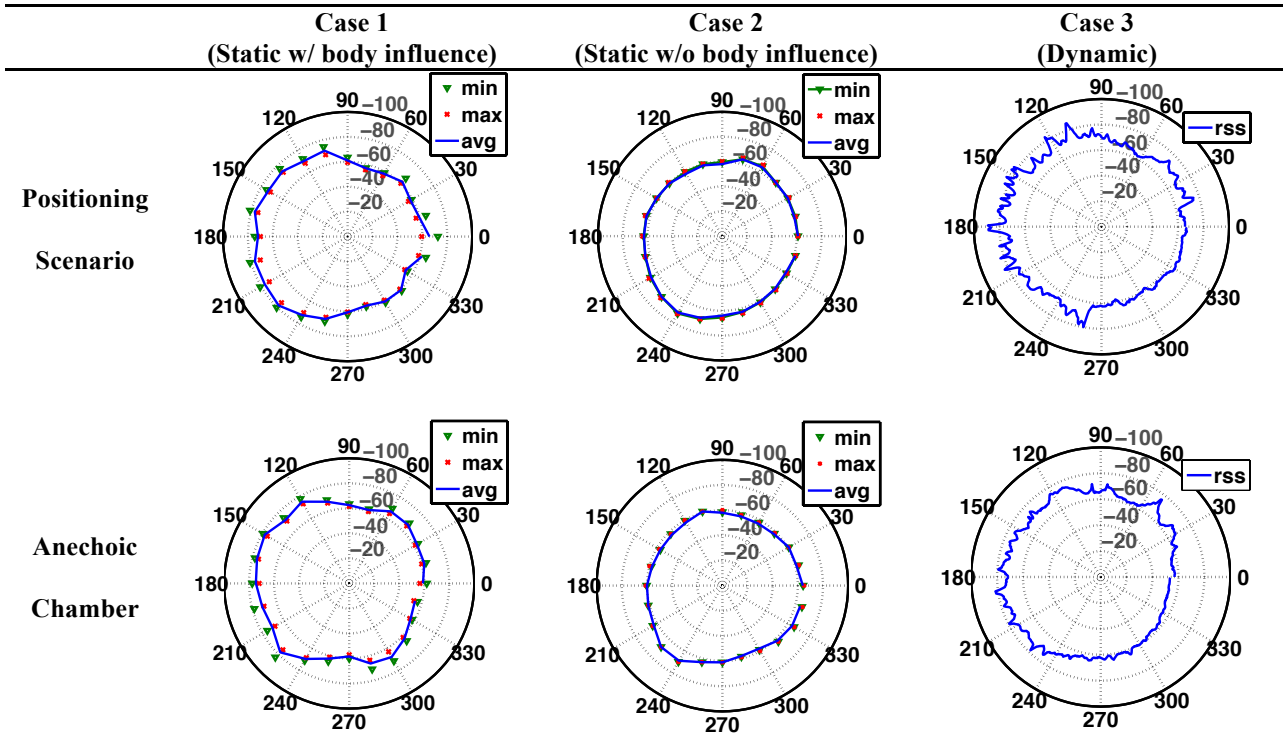

Figure 5: Effect of the human body on the RSS under different scenarios.

There is a clear trend in the plots from Figure 5, where higher RSS attenuation can be seen whenever the body was blocking the LOS. Both scenarios from cases 1 and 3 exhibit this NLOS effect for orientations between 90º and 270º.

The RSS levels depicted in the anechoic chamber and positioning scenarios of case 2 are a function of antenna radiation pattern, antenna placement in the PCB and scenario conditions. There is minimum practical difference between both scenarios in case 2, implying that, for our positioning scenario, the 2-meter minimum distance from the wall was sufficient for signals reflecting of the walls not to be detected by the receiver, and thus not influencing the positioning algorithm error. These reflections are dependent on wall material, which has been studied in works such as [39] and is outside the scope of this work.

The RSS variance increased significantly in case 3 when compared with the other cases, due to the user's motion during the test. It is important to note that the RSS variance increased for both scenarios under dynamic conditions. In the case of the positioning scenario, these variations are generally higher.

The body effect data collected does not appear to agree with superposition of attenuation effects, since the attenuation profile observed in static conditions when the body effect was present is not identifiable in the case where the body was not present.

The RSS variance exhibited in the plots from Figure 5 was solely due to the user's body, which was the only source of motion in the experiments. When the user's body was removed from the test scenarios, plots for minimum, maximum and average RSS overlapped, which indicates that no variations occurred.

The data collected from the anechoic chamber scenario was used to create the body attenuation model presented in Figure 6.

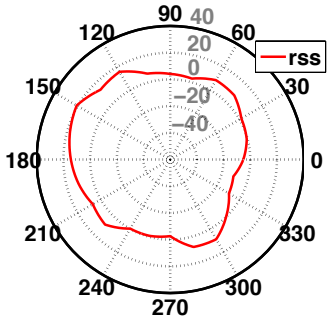

Figure 6: Body attenuation model (units are in dB).

This attenuation model is the result of a combination of multipath and shadowing propagation conditions imposed by the presence of the body inside the anechoic chamber. The model is effectively the difference between the RSS obtained when the body is near the receiving node (case 1) and the RSS obtained when the body effect is not present (case 2).

4.2 Body Effect on the Positioning Algorithm Performance

The body attenuation model obtained in the previous section was used in this section by adding the corresponding RSS attenuation value to the RSS received from each anchor node, according to the angle between the user's orientation and the anchor node direction. These compensated RSS values were then served to the positioning algorithm and a new estimate of position was computed.

In order to experimentally study the body effect in algorithm performance, three sets of data were collected in the positioning scenario. The first set was collected with the sensor node held in the user's hand at approximately 20 cm away from the body (referred to as off-body-20 dataset). The second set was collected with a distance between body and sensor node of 10 cm (referred to as off-body-10 dataset). The last set was collected with the sensor node attached to the user's body at waist level using a Velcro strap (referred to as on-body dataset). These datasets were served as inputs to the WCL and CLP algorithms, generating output estimates without the body effect compensation (WCL and CLP), with the body effect compensation using the true position logged during data collection (WCL+B true pos and CLP+B true pos) and with the body effect compensation using WCL to produce the position estimate (WCL+B est pos and CLP+B est pos). Datasets were collected in different days, at approximately the same hour of the day. Algorithm performance for the off-body-20, off-body-10 and on-body datasets is presented in Figure 7, Figure 8 and Figure 9 respectively.

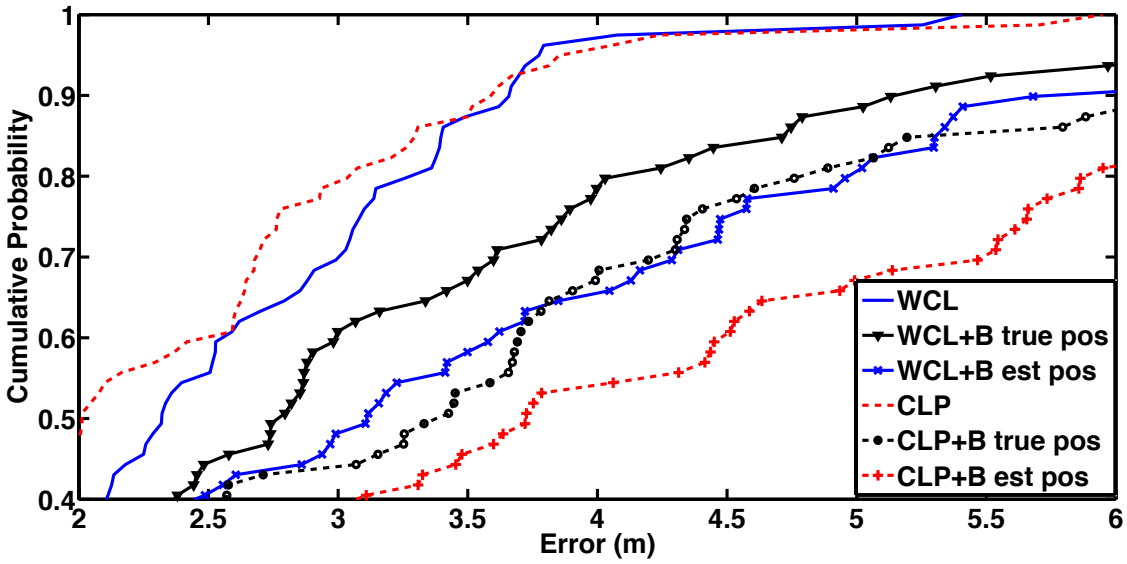

Figure 7: Performance results for the off-body-20 dataset.

The results obtained for the off-body-20 dataset show that the position estimated by each algorithm worsens when the body orientation was accounted, with WCL+B using the true position degrading from 3.03 m to 3.61 m (+19%) compared to WCL, and CLP+B using the true position degrading from 2.69 m to 4.3 m (+59%) compared to CLP, analyzing performances at 70% probability. A lower performance was expected using the estimated position, compared to the true position, when inferring orientation, which is consistent with the results, as can be seen in Figure 7.

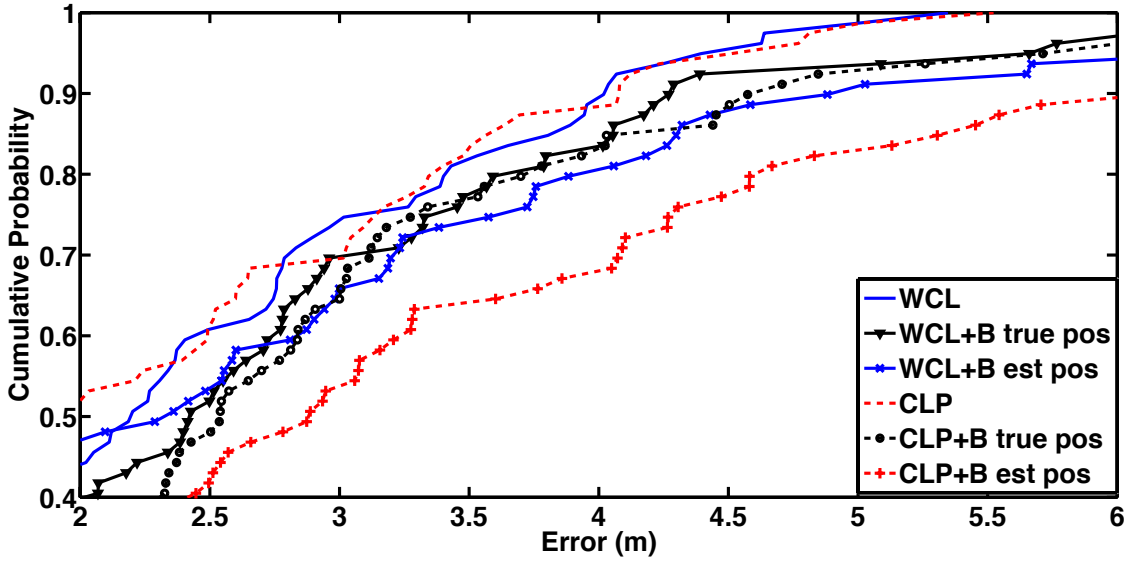

Figure 8: Performance results for the off-body-10 dataset.

The off-body-10 dataset also consistently presented worse performance when accounting body orientation, yet with lesser impact than in previous dataset. WCL+B using the true position degraded from 2.83 m to 3.22 m (+13%) compared to WCL, and CLP+B using the true position produced slightly worse results, from 3.02 m to 3.12 m (+3%), compared to CLP, when analyzing performance at 70% probability. Using the estimated position to infer orientation had lesser impact in performance for this dataset, compared to the previous dataset, although still presenting worse performance. WCL actually performed

better in the off-body-10 dataset than in the off-body-20 dataset, which was contrary to our expectations. The algorithms that account for the body effect improved when compared to their performances in the previous dataset, yet still presenting worse performance than the simpler versions that don't account the body influence.

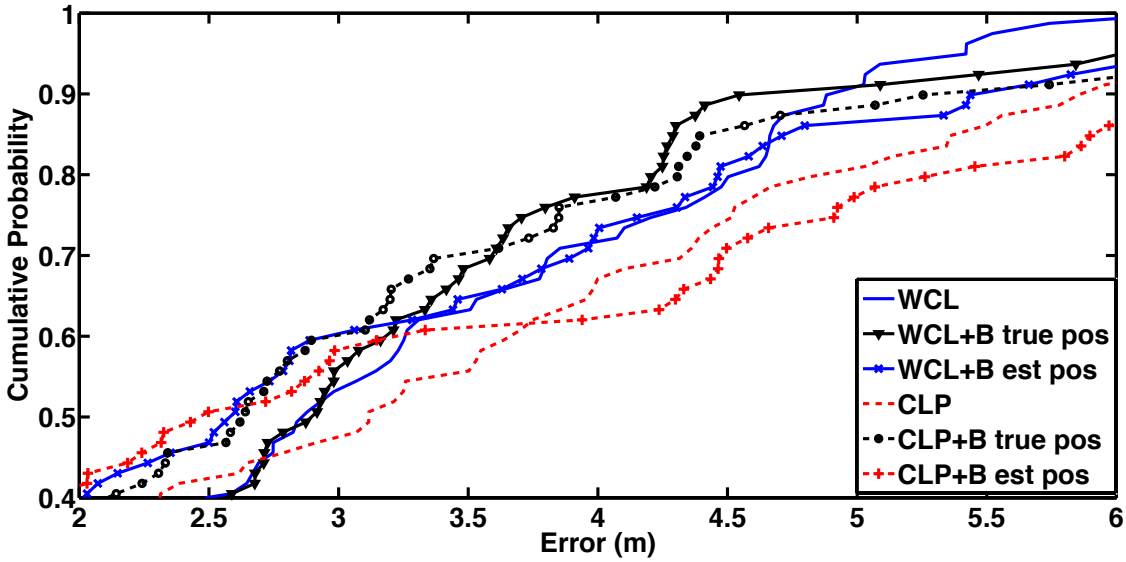

Figure 9: Performance results for the on-body dataset.

Results for the on-body dataset scored the lowest positioning accuracy from all datasets. On the other hand, there were improvements when comparing individually each algorithm with its body effect counterpart, with WCL+B using the true position improving from 3.85 m to 3.6 m (-6%) compared to WCL, and CLP+B improving from 4.36 m to 3.61 m (-17%) compared to CLP, at 70% probability. Using the estimated position for the body effect compensation did not improve the location estimates obtained by WCL and CLP algorithms.

Overall, for the off-body-20, off-body-10 and on-body datasets, CLP (with an accuracy of 2.69 m, an improvement of 11% compared to WCL), WCL (with an accuracy of 2.83 m) and WCL+B using the true position (with an accuracy of 3.6 m, an improvement of 6% compared to WCL), respectively, presented the highest accuracy marks under our test conditions at 70% probability. When comparing WCL and CLP to their counterparts that account the body influence using the estimated position, which is the real use case scenario, the body attenuation model consistently worsened the accuracy. On-body dataset showed lesser degradation of accuracy (in the order of 3%), off-body-10 showed average degradation of accuracy (14% and 35% for WCL and CLP respectively) and off-body-20 showed higher degradation of accuracy (42% and 105% for WCL and CLP respectively). Results are summarized in Table 1.

Table 1: Algorithm performance results for 70% cumulative probability.

	WCL	WCL+B true pos	WCL+B est pos	CLP	CLP+B true pos	CLP+B est pos
Off-Body-20	3.03m	3.61m	4.31m	2.69m	4.3m	5.53m
Off-Body-10	2.83m	3.22m	3.23m	3.02m	3.12m	4.09m
On-Body	3.85m	3.6m	3.96m	4.36m	3.61m	4.49m

In Figure 10, Figure 11 and Figure 12, the geographical distribution of the positioning error is presented for each algorithm, with respect to the off-body-20, off-body-10 and on-body datasets, respectively. The tests were performed with only one user inside the area. If more users were present, the error distribution would certainly generate different error patterns.

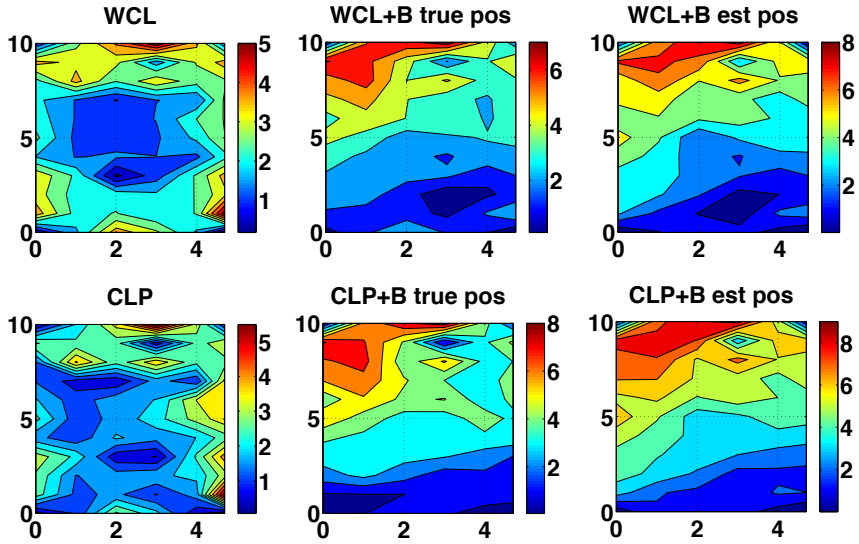

Figure 10: Geographical distribution of positioning error for off-body-20 dataset. Axes are in meters.

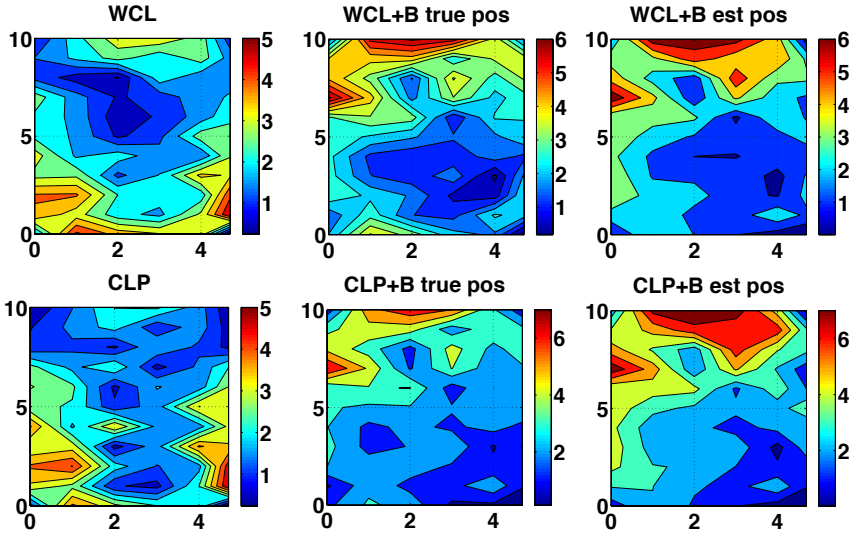

Figure 11: Geographical distribution of positioning error for off-body-10 dataset. Axes are in meters.

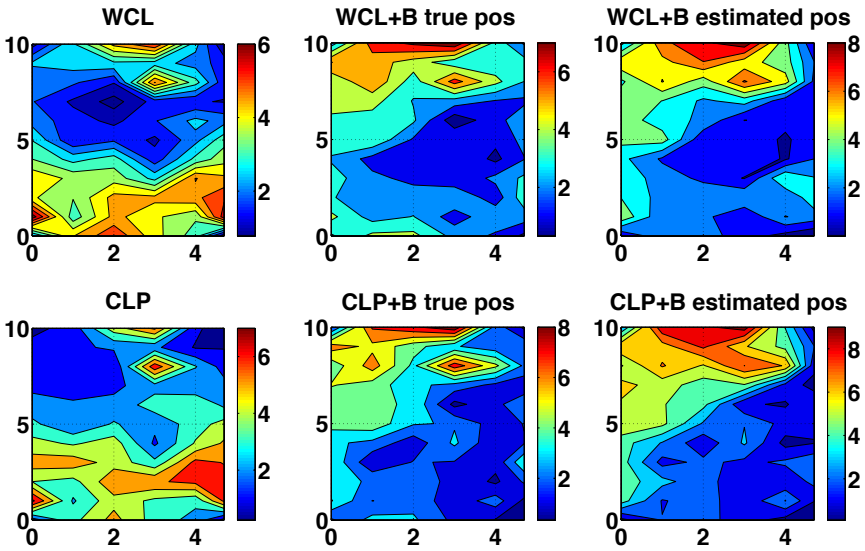

Figure 12: Geographical distribution of positioning error for on-body dataset. Axes are in meters.

It is clear from the geographical error distributions that different positions were subject to different error magnitudes due to the propagation conditions of the scenario. Differences in error distributions were larger between datasets and smaller across positioning algorithms. Overall, the error was generally smaller near an anchor node and larger further away. The center of the positioning area also had a tendency to exhibit lower error.

As a final result presented in this section, we computed the difference between the RSS received by the sensor node and a theoretical RSS that would have been received by the sensor node in ideal conditions, in order to show the RSS deviation from the empirical model that was encountered in the field. Using the real position of the sensor node logged during data collection and the One-Slope model from equation 1, theoretical RSS values for each anchor using the real distances were computed. For this calculation we used the PLE n = 2.19 and P_0 = -37.72 dBm, parameters found using experimental measurements in [15]. The probability distributions (calculated using the *ksdensity* method from MATLAB) for the body attenuation model and the RSS difference for all three datasets are depicted in Figure 13. The body attenuation distribution was also plotted for comparison.

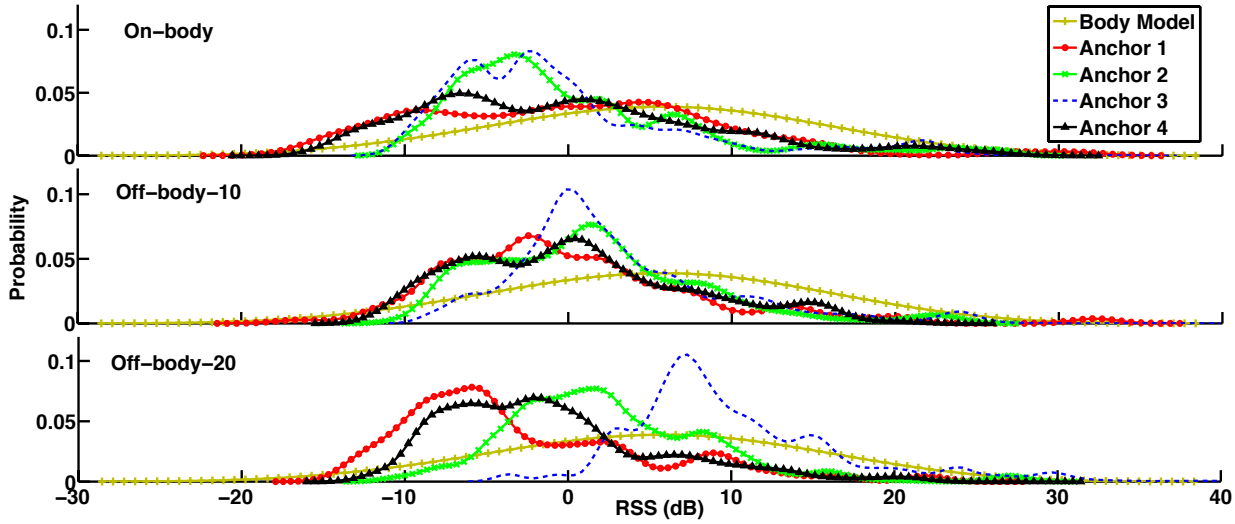

Figure 13: Probability distributions for the difference between real and theoretical RSS received from anchor nodes. Body attenuation model distribution is plotted for comparison.

In the case of the on-body dataset, the distributions of anchors 1 and 4 are similar to the distribution of the body model, which is related to the improvements seen in this dataset when accounting body influence. Distributions for anchors 2 and 3 differ significantly from the body model, meaning that while anchors 1 and 4 are generally correctly compensated using the body model, anchors 2 and 3 deteriorate the distance estimate. For the off-body-10 and off-body-20 datasets, differences between the model and anchors are bigger, which explain why the body influence compensation produced worse results compared to not accounting body influence. It can also be seen that RSS difference is more closely approximated by tailed distributions, rather than Gaussian, as is generally assumed due to the central limit theorem.

5 Discussion

In a previous work [15], the WCL algorithm was tested with and without body influence in the same positioning scenario as in this work, and the performance was improved from 4.0 m to 1.8 m (for a 70% probability) when the body was removed from the scenario, a 55% improvement in position accuracy. Body influence in RSS is widely known to induce error in the position estimation. Accounting for body influence, such as in [40], provided a major impact, improving location estimates. In order to remove or minimize this bias effect caused by the body in [15], we experimented with a body attenuation model in the same positioning scenario.

Considering the best-case scenario (when the body attenuation model was applied using the true position to estimate orientation), only minor improvements on the positioning error were obtained for the on-body dataset. For the datasets where the sensor node is distanced from the body, the body attenuation model consistently deteriorated the performance. This could be explained due to the model being created using on-body data and, as such, it was more likely to produce better results when applied to the on-body dataset. However, this best-case scenario cannot be used in a real use-case (which would use the estimated position to infer orientation), since the body attenuation model consistently deteriorates accuracy in all

datasets, despite the controlled environment with only the user in the positioning area. These results suggest that the shadowing and multipath components caused by the body plays a minor role in the RSS when compared to the multipath component imposed by the environment. The higher body attenuation found in the positioning scenario also stands in agreement with this suggestion.

The distance from the sensor node to the user's body is an important parameter, as evidenced by the differences in performance between datasets. The closer the sensor node is to the body, the worse the positioning algorithms performed in general. The multipath and shadowing component that originates from the body presence is intensified with the inverse of the distance between the body and the receiving antenna, reducing the accuracy achieved by the positioning algorithms tested.

The PLE estimation method used in the CLP algorithm explores the fact that the anchor nodes are configured with their own location. This enables the use of inter-anchor node RSS and distance information in the PLE estimation. The CLP algorithm achieved its highest positioning accuracy of 2.69 m in the off-body-20 dataset, an improvement of 11% compared to WCL. The additional RSS information transmitted in the beacon messages sent by anchor nodes used in the CLP algorithm increased the overhead significantly. However, the algorithm performance has not improved with this added information for the case of the on-body dataset, which is the use-case of interest for a personal positioning system. Given the result obtained for the off-body-20 dataset for the CLP, this PLE estimation method could also outperform the raw RSS used in WCL if the human body was not present in the scenario. These results show that there is a weak correlation between RSS and distance in our indoor environment, where RSS more closely resembles a proximity inference metric than a distance inference metric. These results are also specific to the IEEE 802.15.4 physical layer in the 2.4 GHz frequency band, which is the protocol implemented by the CC2530 hardware modules used in this work.

Using more anchor nodes is a solution to improve localization accuracy; yet, to increase anchor number in our test scenario, precautions would be necessary for the following reasons: extra anchors inside the positioning area would not be possible to add since they would need to be at the same height as other anchors, and, as such, would pose an obstacle to the user inside the positioning area; increasing the number of anchor nodes would increase complexity and the overhead in CLP would grow exponentially.

The distance between anchor nodes and walls is another important parameter to consider when deploying RSS positioning systems. Using a minimum distance of 2 meters from walls, the RSS collected by the sensor node in the positioning setup is approximately the same as the RSS collected in the anechoic chamber. The anchors in our positioning scenario had much lower distances from walls, with 0.36 m in the worst case, and 1.8 m in the best case [15]. These smaller distances affect especially anchors 2 and 3, for which the RSS distributions from Figure 13 differed significantly from other anchors. Further testing would be necessary to find an optimum wall distance that maximizes the efficient use of an indoor space with minimal impact in algorithm performance. The height of the anchor and sensor node with respect to the ground is also an

important parameter, which was made constant in this work. The height influences the ground reflected wave, which can add constructively or destructively to the direct path wave, greatly influencing the RSS.

6 Conclusions and Future Work

It is a fact that the body presence heavily affects the RSS of transmitted messages. Accounting for body influence is consequently seen as a possible solution, capable of bringing major improvements to RSS based positioning algorithm performance. The attenuation model however did not improve positioning algorithm performance under our indoor test scenario. Three datasets with different distances between the body and the sensor node were collected and experimented, and the importance of this distance parameter was highlighted. The results suggest that the multipath propagation effect is more intense when the body is closer to the sensor node. This undermined the performance of the attenuation model used to compensate RSS readings in scenarios where nodes are near or attached to the human body. Positioning algorithm performance degraded as the body approaches the antenna in our test conditions.

A PLE estimation method (CLP) was experimented. This method provided better accuracy than WCL when the body is further apart from the antenna. When the body is closer to the antenna, this improvement is lost and the algorithm performance degraded compared to WCL.

As future work, a Pedestrian Dead Reckoning (PDR) system will be implemented using the sensors from the IMU. The goal is to monitor the user's steps and, in combination with the RSS positioning, allow inferring the distance to anchor nodes with increased accuracy. Furthermore, we intend to integrate the PDR and RSS systems without resorting to computationally intensive algorithms, such as Kalman filters, which are the typical solution.

7 Acknowledgments

This work has been supported by FCT (Fundação para a Ciência e Tecnologia) in the scope of the project UID/EEA/04436/2013. Helder D. Silva is supported by FCT under the grant SFRBD/78018/2011.

8 References

[1] M. Elkhodr, S. Shahrestani, and H. Cheung, 'The Internet of Things: Vision & challenges', *IEEE 2013 Tencon - Spring*, pp. 218–222, Apr. 2013.

[2] M. Weiser, 'The computer for the 21st century', *Scientific american*, vol. 3, no. 3, pp. 94–104, 1991.

[3] L. Atzori, A. Iera, and G. Morabito, 'The Internet of Things: A survey', *Computer Networks*, vol. 54, no. 15, pp. 2787–2805, Oct. 2010.

[4] IEEE, 'Standard for Local and metropolitan area networks - Part 15.4: Low-Rate Wireless Personal Area Networks (LR-WPANs)', 2011.

[5] E. Miluzzo, X. Zheng, K. Fodor, and A. T. Campbell, 'Radio Characterization of 802.15.4 and Its Impact on the Design of Mobile Sensor Networks', in *5th European Conf. on Wireless Sensor Networks (EWSN '08)*, 2008, pp. 171–188.

[6] F. Della Rosa, M. Pelosi, and J. Nurmi, 'Human-induced effects on RSS ranging measurements for cooperative positioning', *International Journal of Navigation and Observation*, vol. 2012, pp. 1–13, 2012.

[7] A. Awad, T. Frunzke, and F. Dressler, 'Adaptive Distance Estimation and Localization in WSN using RSSI Measures', in *10th Euromicro Conference on Digital System Design Architectures, Methods and Tools (DSD 2007)*, 2007, no. Dsd, pp. 471–478.

[8] C. Savarese, J. Rabaey, and K. Langendoen, 'Robust Positioning Algorithms for Distributed Ad-Hoc Wireless Sensor Networks', in *ATEC '02 Proceedings of the General Track of the annual conference on USENIX Annual Technical Conference*, 2002, pp. 317–327.

[9] IEEE, 'IEEE Std 802.15.4a-2007: Wireless MAC and PHY Specifications for LR-WPANs - Amendment 1: Add Alternate PHYs', 2007.

[10] G. V. Zàruba, M. Huber, F. a. Kamangar, and I. Chlamtac, 'Indoor location tracking using RSSI readings from a single Wi-Fi access point', *Wireless Networks*, vol. 13, no. 2, pp. 221–235, Jun. 2006.

[11] C. Oliveira and L. M. Correia, 'A Statistical Model to Characterize User Influence in Body Area Networks', *Vehicular Technology Conference Fall (VTC 2010-Fall), 2010 IEEE 72nd*. pp. 0–4, 2010.

[12] M. Mackowiak and L. Correia, 'Towards a Radio Channel Model for Off-Body Communications in a Multipath Environment', in *18th European Wireless Conference European Wireless*, 2012.

[13] A. Goldsmith, *Wireless Communications*. Cambridge University Press, 2005.

[14] J. Wilson and N. Patwari, 'See Through Walls: Motion Tracking Using Variance-Based Radio Tomography Networks', *IEEE Transactions on Mobile Computing*, vol. 10, no. 5, pp. 612–621, 2011.

[15] H. Silva, J. Afonso, and L. Rocha, 'Experimental Performance Comparison of Indoor Positioning Algorithms Based on Received Signal Strength', in *Proceedings of the World Congress of Engineering*, 2014, vol. I, pp. 677–683.

[16] R. C. Luo, O. Chen, and C. W. Lin, 'Indoor Human Monitoring System Using Wireless and Pyroelectric Sensory Fusion System', in *The 2010 IEEE/RSJ International Conference on Intelligent Robots and Systems*, 2010, pp. 1507–1512.

[17] P. Tarrío, M. Cesana, and A. Redondi, 'Energy-accuracy trade-offs for hybrid localization using RSS and inertial

measurements in wireless sensor networks', *Ad Hoc Networks*, vol. 11, no. 6, pp. 1874–1889, Aug. 2013.

[18] T. Gadeke, J. Schmid, W. Stork, and K. D. Muller-Glaser, 'Pedestrian Dead Reckoning for Person Localization in a Wireless Sensor Network', in *International Conference on Indoor Positioning and Indoor Navigation*, 2011, no. September.

[19] J. Blumenthal, R. Grossmann, F. Golatowski, and D. Timmermann, 'Weighted Centroid Localization in Zigbee-based Sensor Networks', *2007 IEEE International Symposium on Intelligent Signal Processing*, pp. 1–6, 2007.

[20] F. Reichenbach and D. Timmermann, 'Indoor Localization with Low Complexity in Wireless Sensor Networks', *2006 IEEE International Conference on Industrial Informatics*, pp. 1018–1023, Aug. 2006.

[21] Z. Zhang, G. Wan, M. Jiang, and G. Yang, 'Research of An Adjacent Correction Positioning Algorithm Based on RSSI-Distance Measurement', in *2011 Eighth International Conference on Fuzzy Systems and Knowledge Discovery (FSKD)*, 2011, pp. 2319–2323.

[22] M. B. Zeytinci, V. Sari, F. K. Harmanci, E. Anarim, and M. Akar, 'Location estimation using RSS measurements with unknown path loss exponents', *EURASIP Journal on Wireless Communications and Networking*, pp. 1–14, 2013.

[23] P. Bahl and V. N. Padmanabhan, 'RADAR: An In-building RF-based User Location and Tracking System', in *INFOCOM 2000. Nineteenth Annual Joint Conference of the IEEE Computer and Communications Societies. Proceedings. IEEE*, 2000, vol. 2, pp. 775 – 784 vol.2.

[24] J. Machaj, R. Piché, and P. Brida, 'Rank Based Fingerprinting Algorithm for Indoor Positioning', in *International Conference on Indoor Positioning and Indoor Navigation*, 2011, no. September, pp. 1–6.

[25] P. Mestre, C. Serodio, L. Coutinho, L. Reigoto, and J. Matias, 'Hybrid technique for fingerprinting using IEEE802.11 wireless networks', in *2011 International Conference on Indoor Positioning and Indoor Navigation, IPIN*, 2011, no. September, pp. 1–7.

[26] M. Veletić and M. Šunjevarić, 'On the Cramer-Rao lower bound for RSS-based positioning in wireless cellular networks', *AEU - International Journal of Electronics and Communications*, vol. 68, no. 8, pp. 730–736, Aug. 2014.

[27] M. Kochlan and J. Micek, 'Indoor Propagation of 2.4 GHz Radio Signal: Propagation Models and Experimental Results', in *The 10th International Conference on Digital Technologies*, 2014, pp. 125–129.

[28] T. S. Rappaport, *Wireless Communications: Principles and Practice*. Englewood Cliffs, New Jersey: Prentice-Hall, 1996.

[29] M. F. Iskander, 'Propagation prediction models for wireless communication systems', *IEEE Transactions on Microwave Theory and Techniques*, vol. 50, no. 3, pp. 662–673, Mar. 2002.

[30] N. Patwari, J. N. Ash, S. Kyperountas, A. O. Hero, R. L. Moses, and N. S. Correal, 'Locating the nodes: cooperative localization in wireless sensor networks', *IEEE Signal Processing Magazine*, vol. 22, no. 4, pp. 54–69, Jul. 2005.

[31] Y. Qi, ‘Wireless Geolocation in a Non-Line-of-Sight Environment’, Princeton University, 2003.

[32] S. Mazuelas, A. Bahillo, R. M. Lorenzo, P. Fernandez, F. a. Lago, E. Garcia, J. Blas, and E. J. Abril, ‘Robust Indoor Positioning Provided by Real-Time RSSI Values in Unmodified WLAN Networks’, *IEEE Journal of Selected Topics in Signal Processing*, vol. 3, no. 5, pp. 821–831, Oct. 2009.

[33] C. Gentile, N. Alsindi, R. Raulefs, and C. Teolis, *Geolocation Techniques*. Springer, 2013.

[34] D. Sanchez, M. a. Quintana, and J. L. Navarro, ‘WLAN Location Determination Using Probability Distributions with Search Area Reduction via Trilateration’, *2009 Fifth International Conference on Wireless and Mobile Communications*, no. 1, pp. 328–333, 2009.

[35] F. Della Rosa, L. Xu, H. Leppäkoski, and J. Nurmi, ‘Relative Positioning of Mass Market Devices in Ad-hoc Networks’, in *International Conference on Indoor Positioning and Indoor Navigation*, 2011, no. September.

[36] J. Palazon, J. Gozálvez, and G. Prieto, ‘Experimental RSSI-based localization system using wireless sensor networks.’, *17th IEEE International Conference on Emerging Technologies and Factory Automation*, 2012.

[37] Antenova, ‘Titanis 2.4 GHz Swivel SMA Antenna Product Specification’, 2015.

[38] P. Macedo, J. Afonso, L. Rocha, and R. Simões, ‘A telerehabilitation system based on wireless motion capture sensors’, in *International Conference on Physiological Computing Systems, PhyCS 2014*, 2014, pp. 55–62.

[39] E. Damosso and L. M. Correia, ‘Cost Action 231: Digital Mobile Radio Towards Future Generation Systems, Final Report.’, 1999.

[40] F. Della Rosa, L. Xu, J. Nurmi, C. Laoudias, M. Pelosi, and A. Terrezza, ‘Hand-grip and body-loss impact on RSS measurements for localization of mass market devices’, *2011 International Conference on Localization and GNSS (ICL-GNSS)*, pp. 58–63, 2011.